ISSN 0965-545X, Polymer Science, Series A, 2016, Vol. 58, No. 6, pp. 886–898. © Pleiades Publishing, Ltd., 2016.

IN MEMORY
OF PROFESSOR EDWARDS

Theory of Heterogeneities in Polymer Networks[1]

S. V. Panyukov*

Theoretical Department, P. N. Lebedev Physical Institute, Russian Academy of Sciences, Moscow, 117924 Russia
**e-mail: panyukov@lpi.ru*

Received October 19, 2015;
Revised Manuscript Received April 20, 2016

Abstract—Following Edwards' ideas we present main experimental results and the theory of random heterogeneities in neutral and charged networks obtained by instantaneous as well as chemical cross-linking of a melt and semidilute solution of linear chains. We study how random monomer density patterns in such networks change after swelling and stretching. We also describe main features of monomer density correlation functions, which determine the neutron and light scattering on spatial heterogeneities. We show that large-scale cross-link density patterns written into network structure in the melt or semidilute state, can be revealed upon swelling by monitoring the monomer density patterns. We demonstrate that while isotropic deformations in good solvent yield magnified images of the original pattern, anisotropic deformations distort the image. We study how the monomer density image changes under different solvent conditions and discuss the difference between deformations of the density images in gels and ordinary solids. Possible tests of our predictions and some potential applications are proposed.

DOI: 10.1134/S0965545X16060158

INTRODUCTION

Sam Edwards started his research in PhD on the structure of the electron using techniques of quantum field theory. Later, he realized that he could apply the field theory methods outside particle physics to solve many complex problems in condensed matter physics and polymers. Over the course of nearly half a century, using such advanced techniques Sam Edwards has led polymer science into one of the most developed directions of physics. He published seminal papers on the statistical mechanics of polymers with excluded volume [1], the theory of polymer solutions at intermediate concentration [2] and statistical mechanics with topological constraints [3].

In the classical tube model, proposed by Edwards [4] for polymer networks with strongly entangled linear strands, each strand is confined by its neighbors to a tube-like region. In collaboration with M. Doi [5, 6] he introduced the reptation process to the theory of polymer dynamics: entangled long chain molecules diffuse as if they were confined to the entangled tube. Employing the technique known as the replica trick he proposed [7] a new approach to the description of thermodynamics of polymer networks. To those who came after him, Sam Edwards gave very efficient tool for further researches.

Many polymer networks and gels display inhomogeneity of their cross-linking density, along with additional topological defects such as dangling chain ends, cross-linker shortcuts, and chains forming loops. The origin of this heterogeneity and its characterization by light, neutron, and X-ray scattering as well as by NMR spectroscopy and optical, electron, and X-ray microscopies is reviewed in [8]. First attempts to take such heterogeneities into account were made by using the model of randomly cross-linked networks containing fractal regions, such as regular Sierpinski gaskets [9] and percolation clusters [10]. In [11] it is shown that the fractal heterogeneities yield extra contributions to the deformation process since such networks can be swollen and deformed by defolding the fractal regions without significant elastic entropy penalty.

The defolding of long strands in a network is limited by their entanglements. The effect of entanglements on heterogeneities in polymer networks is studied in [12] using molecular dynamics simulations of polymer networks made by either end-linking or randomly crosslinking a melt of linear precursor chains. The end-linking leads to nearly ideal monodisperse networks, while random cross-linking produces strongly polydisperse networks. The main conclusion of this work is that the microscopic strain response, diameter of the entanglement tube, and stress–strain relation are all insensitive to the heterogeneities due to the linking process by which the networks were made.

Dynamic response of inhomogeneous polymer network modeled as an assembly of noninteracting crosslinked regions (domains) of various sizes is stud-

[1]The article is published in the original.

ied in [13]. It is shown that the averaging over different domain sizes can significantly change time dependence of the relaxation modulus of the polymer network. In case of exponential size distribution it follows a stretched exponent law, whilst the theory predicts a power-law time dependence for regular polymer networks.

The Edwards replica trick is widely used to describe polymer networks, both physical [14] (in equilibrium with respect to bond breakage and formation) and chemical (with fixed topological structure) [15]. The replica method is applied in Ref. [16] to develop the density functional approach to describe networks formed by random cross-linking a melt of polymer chains. The characteristic size and amplitude of the spatial nonuniformities of the network due to defects of its structure and topological restrictions are calculated in [17]. The replica approachis also used to show that inhomogeneities can arise as consequences of a stretching of polymer networks [18].

Following Edwards' ideas, in [19] we performed a comprehensive statistical mechanical analysis of the Edwards model of gels, formed by chemical cross-linking of semi-dilute polymer solutions. Although this theory provides a complete solution of the statistical mechanics of polymer gels, it uses replica trick which is unfamiliar to the majority of people in the polymer community. A more intuitive phenomenological approach capturing all the main physical ingredients of the complete theory is developed in [20].

In this work, we apply this approach to study spatial heterogeneities developed in swollen and deformed polymer networks. The non-triviality of this problem stems from the fact that information about network structure is "encrypted" in the pattern of cross-links joining polymer chains, which represent very small fraction of the network volume. The memorization of initial cross-link pattern is, however, only partial, as a result of the thermal fluctuations that occur in the new, post-cross-linking equilibrium state. Conformations of polymer strands in such networks with fixed topological structure can be varied in a wide range depending on experimental conditions, so polymer networks can be significantly deformed without irreversible damage to their structure.

Below we outline a theory of polymer gels which accounts for the frozen inhomogeneity of their structure, as well as for the fact that gels behave as solids on large scales and as liquids on small scales (smaller than the length scale of monomer fluctuations in the network). We demonstrate that this theory reproduces all the qualitative features observed in neutron and light scattering experiments on neutral and charged gels.

One of the main questions to which we answer in our work is: what information can be "written" in cross-link pattern, and under what conditions it can be "read" back? Once a homogeneous (on length scales large compared to its "mesh" size) network is formed, one can generate large-scale patterns in it by further cross-linking, followed by swelling (and possibly stretching) of the network, resulting in a gel inhomogeneously swollen by solvent. This can be done, for example, by adding light-sensitive cross-links to a transparent network. Focusing a laser beam in regions inside the gel one can "write" information into gel structure in the form of 2D or 3D patterns of cross-linking density. In this paper we show that although such information is hidden at preparation conditions, it can be recovered by swelling the gel since unobservable variations of cross-link density in the melt are transformed into observable variations of monomer density in the swollen gel.

Regions of a gel with increased cross-link concentration can be considered as inclusions with enhanced elastic modulus, see Fig. 1a. If such inclusions deform differently from polymer matrix, as in case of any normal elastic solids, they would induce elastic stresses in the gel and initial pattern would be significantly distorted due to long range character of elastic interactions, see Fig. 1b. This scenario determines, for example, the elastic properties of amorphous polycrystalline solids but it does not apply to polymer gels, because of the unusual character of gel elasticity. We show that in swollen gels that are isotropically stretched by absorption of solvent, the observed monomer density pattern is not distorted and is simply an affinely stretched variant of the initial cross-linking pattern, see Fig. 1c. Such gels can serve as a magnifying glass that enlarge the initially written pattern without distorting its shape. The corresponding magnification factor can be very large in case of super-elastic networks.

THERMODYNAMICS OF RANDOM HETEROGENETIES

We consider networks formed by cross-linking a melt or a semidilute solution of polymer chains. Due to the randomness of the cross-linking process the structure of such a network is strongly irregular. Upon network swelling density heterogeneities appear which can be imaged on a light-sensitive screen. The so-called "speckle patterns" observed in such experiments remain unchanged for a few hours and days, see Inset in Fig. 2. In this section we develop thermodynamic description of random heterogeneities in polymer networks. To understand how such random density patterns depend on network structure we consider networks synthesized at different preparation conditions: in a melt as well as in semidilute polymer solutions, cross-linked both instantaneously and at equilibrium conditions. In case of instantaneous cross-linking, one begins with the melt or solution at equilibrium and—so rapidly that hardly any relaxation has time to occur—one introduces permanent bonds between some random fraction of the pairs of chain segments that happen, at the instant of cross-linking,

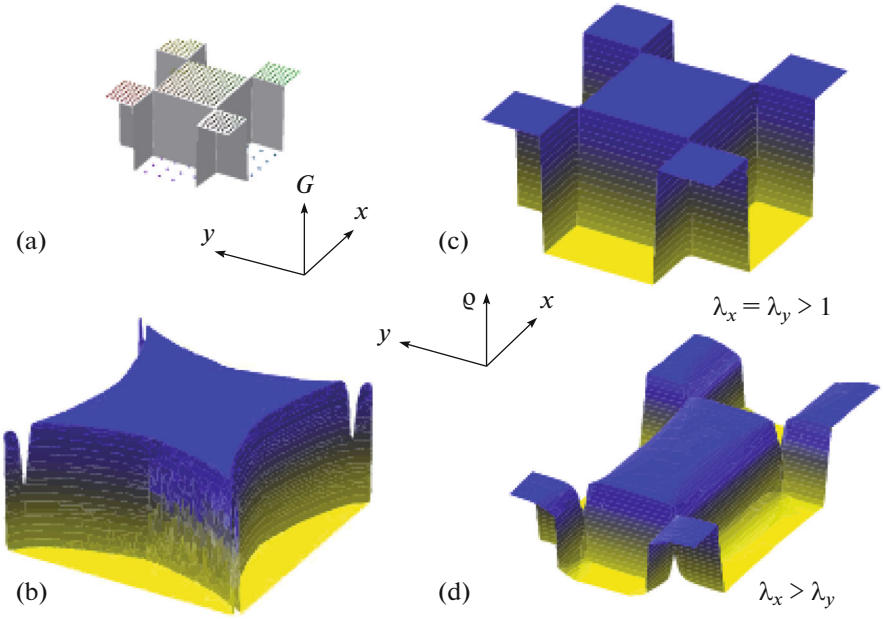

Fig. 1. (Color online) (a) Elastic modulus profile in undeformed solid. Density profile in isotropically deformed solids; (b) In normal elastic solid softer regions at edges deform more than rigid regions in the central area; (c) polymer networkis isotropically stretched by factors $\lambda_1 = \lambda_2 = 1.5$; and (d) anisotropically stretched by factors $\lambda_1 = 2$, $\lambda_2 = 1$.

to be nearby one another. In case of chemical cross-linking one can "freeze" the instantaneous configuration of reversible bonds between chains in equilibrium polymer melt or solution using single-pulse ultraviolet laser excitation or quickly lowering the temperature.

Elastic Free Energy of Network with Heterogeneities

We first study gel structure on macroscopic length scales far exceeding the radius of monomer fluctuations R (or, alternatively, the average mesh size of the undeformed network), when the network can be treated as a (soft) elastic solid. Elastic deformation of a solid can be described by deformation gradient tensor $\mathbf{F}$ with components

$$F_{kl} = \frac{\partial x_k}{\partial x_{0l}}, \quad (1)$$

where $\mathbf{x}_0$ and $\mathbf{x}$ are coordinates of the same material point in preparation and in deformed state of the gel. It is convenient to assume that the gel is deformed with respect to preparation state in two stages:

$$F_{kl} = \Sigma_j F^u_{kj} F^{\text{ref}}_{jl} \quad (2)$$

Thus, the gel is first stretched with respect to its preparation state by factors λ_k along axes $k = x, y, z$. Since coordinates of such a reference state $\mathbf{x} = \lambda\mathbf{x}_0$ deform affinely (with components $x_k = \lambda_k x_{0k}$), we get the gradient tensor and the monomer density in this state

$$F^{\text{ref}}_{jl} = \lambda_j \delta_{jl}, \quad \rho^{\text{ref}}(\mathbf{x}) = \rho_0(\boldsymbol{\lambda}^{-1} \cdot \mathbf{x})/(\lambda_x\lambda_y\lambda_z), \quad (3)$$

where $\rho_0(\mathbf{x}_0)$ is monomer density in the undeformed preparation state. Even though such affinely deformed state does not minimize the free energy and therefore is not an equilibrium state of the deformed gel, we use it as a reference state.

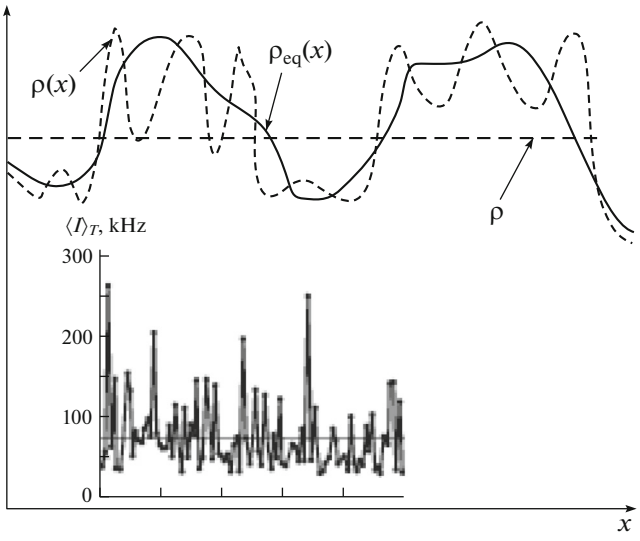

Fig. 2. Instant monomer density profile $\rho(\mathbf{x})$ in polymer networks (dotted line) and different averages: $\rho_{eq}(\mathbf{x}) = \langle\rho(\mathbf{x})\rangle$ is thermodynamic average (over time intervals, solid line) and $\bar{\rho} = \overline{\langle\rho(\mathbf{x})\rangle}$ is statistical average (over space). The amplitude of frozen heterogeneities is defined as $\Delta\rho(\mathbf{x}) = \rho_{eq}(\mathbf{x}) - \bar{\rho}$, the amplitude of thermal fluctuations is $\delta\rho(\mathbf{x}) = \rho(\mathbf{x}) - \rho_{eq}(\mathbf{x})$. The inset shows a typical experimentally observed dependence of the time-averaged scattering amplitude at a given angle $\langle I \rangle_T$ on the position of the sample (speckle pattern).

The true equilibrium state of the deformed network has an inhomogeneous monomer density profile and is defined by introducing a displacement field $\mathbf{u}(\mathbf{x})$ defined with respect to the above reference state:

$$\mathbf{x}' = \mathbf{x} + \mathbf{u}(\mathbf{x}) \tag{4}$$

and we get gradient tensor and monomer density of the equilibrium state as function of coordinates $\mathbf{x}$ of the reference state

$$F_{kl}^{u} = \delta_{kl} + \frac{\partial u_k}{\partial x_l}, \quad \rho(\mathbf{x}) = \frac{\rho^{\text{ref}}(\mathbf{x})}{\det(\mathbf{F}^u)}, \tag{5}$$

$$\det(\mathbf{F}^u) \cong 1 + \Sigma_k \frac{\partial u_k}{\partial x_k}. \tag{6}$$

Following the classical theories of gel elasticity [20, 21] the gel free energy can be written as:

$$A = \int\left(\frac{G(\mathbf{x}_0)}{2}\Sigma_{kl}F_{kl}^2 + f[\rho(\mathbf{x}_0)]\right)d\mathbf{x}_0. \tag{7}$$

Here $f(\rho)$ is the osmotic (interaction) part of the free energy of the gel, with monomer density ρ. The polymer contribution to the elastic modulus of the cross-linked melt is proportional to the local cross-link density

$$G(\mathbf{x}_0) \cong k_{\text{B}}T\rho_0(\mathbf{x})/N, \tag{8}$$

where N is the number of statistical segments ("monomers") of an average network chain, $k_{\text{B}}T$ is thermal energy, k_{B} is Boltzmann constant and T is temperature.

We now express the free energy, Eq. (7), in terms of the displacement field, referred to the final deformed (and, depending on the deformation, possibly anisotropic) state. For this we need to substitute Eq. (5) into Eq. (7) and introduce the change of variables $\mathbf{x}_0 \to \mathbf{x}$. Under this transformation, the gradient operators in the two states are related by

$$\frac{\partial}{\partial x_{0k}} = \lambda_k \frac{\partial}{\partial x_k}, \tag{9}$$

and the volume element transforms as

$$d\mathbf{x}_0 = d\mathbf{x}/(\lambda_x\lambda_y\lambda_z). \tag{10}$$

In a swollen state the monomer density is small and the interaction energy can be expanded as $f(\rho) \cong k_{\text{B}}TB\rho^2/2$ where B is second virial coefficient. Expanding the free energy in powers of $\mathbf{u}$ and integrating over the volume of the undeformed network we get

$$\Delta A = \int\left[\hat{G}(\lambda^{-1}\cdot\mathbf{x})\Sigma_k\lambda_k^2\frac{\partial u_k}{\partial x_k} + \frac{\overline{G}}{2}\Sigma_{kl}\left(\lambda_l\frac{\partial u_k}{\partial x_l}\right)^2 + \frac{K^{\text{os}}}{2}\left(\Sigma_k\frac{\partial u_k}{\partial x_k}\right)^2\right]\frac{d\mathbf{x}}{\lambda_x\lambda_y\lambda_z}, \quad K^{\text{os}} = k_{\text{B}}TB\overline{\rho}^2. \tag{11}$$

Here $\hat{G}(\mathbf{x}_0)$ represents the variations of cross-link density,

$$G(\mathbf{x}_0) = \overline{G} + \hat{G}(\mathbf{x}_0). \tag{12}$$

The term with constant modulus $\overline{G}$ upon integration contribute a surface term which balances the externally applied force.

In the Fourier representation, the free energy associated with deformations and fluctuations about the affinely deformed state can be rewritten as

$$\Delta A = \int\frac{d\mathbf{q}}{(2\pi)^3}\left[-\tilde{\mathbf{f}}(-\mathbf{q})\tilde{\mathbf{u}}(\mathbf{q}) + \frac{1}{2}\tilde{\mathbf{u}}(-\mathbf{q})\tilde{G}(\mathbf{q})\tilde{\mathbf{u}}(\mathbf{q}) + \frac{K^{\text{os}}}{2}|\mathbf{q}\tilde{\mathbf{u}}(\mathbf{q})|^2\right]. \tag{13}$$

The tensor $\tilde{G}(\mathbf{q})$ is a quadratic form in $\mathbf{q}$, the coefficients of which are the elastic moduli of the deformed network (these moduli depend on the extension ratios λ_k) [19]:

$$\tilde{G}_{kl}(\mathbf{q}) = (\boldsymbol{\lambda}\cdot\mathbf{q})^2\overline{G}\delta_{kl}. \tag{14}$$

The tensor of elastic moduli is obtained by dividing the tensor $\tilde{G}_{kl}(\mathbf{q})$ by q^2. We conclude that the modulus of an anisotropically deformed network (for which some of the $\{\lambda_k\}$ differ from each other) depends on the externally imposed deformation and is, in general, anisotropic.

Since the reference state is not an equilibrium state, gel energy in Eq. (13) contains a term linear in $\mathbf{u}$. The random force $\tilde{\mathbf{f}}$ is the source of spatial inhomogeneities. It can be written as a sum of two contributions [20, 21]:

$$\tilde{\mathbf{f}}(\mathbf{q}) = \tilde{\mathbf{f}}^{\text{cr}}(\mathbf{q}) + \tilde{\mathbf{f}}^{\text{rand}}(\mathbf{q}). \tag{15}$$

The cross-link contribution to the force density is given by

$$\tilde{\mathbf{f}}_l^{\text{cr}}(\mathbf{q}) = i\lambda_l^2 k_{\text{B}}Tq_l\rho^{\text{ref}}(\mathbf{q})/N, \tag{16}$$

and its statistical properties are completely defined by those of the density of cross-links in the state of preparation of the network. The random force $\tilde{\mathbf{f}}^{\text{rand}}$ distinguishes between different network structures which have the same density distribution in the preparation state. The correlator of this force associated with the frozen-in fluctuations of network structure in the deformed state is

$$\overline{\tilde{f}_k^{\text{rand}}(\mathbf{q})\tilde{f}_l^{\text{rand}}(-\mathbf{q})} = 3\lambda_k^2(k_{\text{B}}T)^2\frac{\overline{\rho}}{2N}(\boldsymbol{\lambda}\cdot\mathbf{q})^2\delta_{kl}. \tag{17}$$

While the preceding analysis neglects the contribution of entanglements to the elasticity of gels, it can be extended to the case of entangled networks. We consider entanglements using the famous Edwards idea of effective potential representing effective tube. The entanglements give an additional contribution to the elasticity tensor $\tilde{G}(\mathbf{q})$ which can be calculated for arbi-

trary wave vectors $\mathbf{q}$ in the model of nonaffine tube [22, 23]:

$$\tilde{G}^{e}_{kl}(\mathbf{q}) = k_B T \frac{\rho(\boldsymbol{\lambda}\cdot\mathbf{q})^2}{N_e\lambda_k}\frac{1}{4+N_e\lambda_k b^2(\boldsymbol{\lambda}\cdot\mathbf{q})^2/3}\delta_{kl}. \quad (18)$$

N_e is number of monomers between neighboring entanglements and b is monomer size. Since the topological constraints are weakened on small scales, the entanglement modulus quickly decays with q.

Random Heterogeneities

It has been known from experiments that the scattering intensity increases by introducing cross-links due to cross-linking heterogeneities. Stein [24] discovered the heterogeneities in cross-linking rubber by light scattering. Mallam with coworkers [25] observed that the scattering intensity $S(q)$ of polyacrylamide (PAAm) gels with different cross-link concentrations increased with increasing cross-link density. The upturn in $S(q)$ at low wavevectors q is recognized as to be due to the presence of static inhomogeneities, the amplitude of which increases with increasing cross-link density. Below we present theoretical background for the description of random heterogeneities in swollen/deformed gels.

Random inhomogeneous density profile. We refer to the Fourier transform of the deviation from the average monomer density as the "density" distribution, since the latter can be recovered from it by the Fourier transform,

$$\rho_{eq}(\mathbf{x}) = \overline{\rho} + \delta\rho_{eq}(\mathbf{x}) = \overline{\rho} + \int \tilde{\rho}_{eq}(\mathbf{q}) e^{i\mathbf{q}\mathbf{x}} \frac{d\mathbf{q}}{(2\pi)^3}. \quad (19)$$

The equilibrium monomer density profile is given by [21]

$$\tilde{\rho}_{eq}(\mathbf{q}) = \frac{\tilde{n}(\mathbf{q})}{1+B\tilde{g}(\mathbf{q})}. \quad (20)$$

The density profile in the "elastic reference state" [19] $\tilde{n}(\mathbf{q})$ maximizes the entropy of polymer network. The density $\tilde{n}(\mathbf{q})$ vanishes in the short wavelength limit $q \ll R^{-1}$, since there can be no spatial inhomogeneities in a network on length scales smaller than the monomer fluctuation radius R. The radius R depends on the structure of the network under consideration and in the mean field approximation $R \cong bN^{1/2}$, where b is the monomer size [19]. A more general expression for R which applies to the semi-dilute regime will be given later. As can be seen from Eq. (20), the equilibrium density profile is more homogeneous than that of the corresponding elastic reference state.

The thermal structure factor of the gel in Eq. (20) is

$$\tilde{g}(\mathbf{q}) = \overline{\rho}N\left[\frac{1}{Q^2/2+(4Q^2)^{-1}+1} + \frac{2Q^2}{(1+Q^2)^2(\boldsymbol{\lambda}\cdot\mathbf{Q})^2}\right], \quad (21)$$

where $\mathbf{Q} = R\mathbf{q}$ is the dimensionless wavevector normalized by the monomer fluctuating radius. The term $Q^2/2$ in the denominator of the first term of the right hand side of Eq. (21) gives the usual Lifshitz entropy of polymer solutions [26]. The term $(4Q^2)^{-1}$, first introduced by de Gennes for heteropolymer networks [27], describes the suppression of density fluctuations on length scales larger than the monomer fluctuation radius R. The function $\tilde{g}(\mathbf{q})$ retains its angular dependence on the anisotropic deformation, even in the limit $q \to 0$.

Note that there are two types of averages, i.e., the *thermal* or *time averages* and *ensemble* or *space averages*, denoted by $\langle X\rangle$ and $\overline{X}$, respectively. The Fourier component of the thermal correlator of density fluctuations $\delta\rho(\mathbf{x}) = \rho(\mathbf{x}) - \rho_{eq}(\mathbf{x})$ (see Fig. 2) is:

$$\tilde{D}(\mathbf{q}) = \langle|\delta\tilde{\rho}(\mathbf{q})|^2\rangle = \frac{\tilde{g}(\mathbf{q})}{1+B\tilde{g}(\mathbf{q})}. \quad (22)$$

The density in the "elastic reference state" is random value characterized by the correlator

$$v(\mathbf{q}) = \overline{\tilde{n}(\mathbf{q})\tilde{n}(-\mathbf{q})} = \frac{1}{(1+Q^2)^2}\left[6\overline{\rho}N + \frac{9}{\lambda_x\lambda_y\lambda_z}S_0(\boldsymbol{\lambda}\cdot\mathbf{q})\right]. \quad (23)$$

The first term in the brackets comes from the correlator of the force density associated with the frozen-in variations of network structure (see Eq. (17)). The second term in the brackets in Eq. (23) is proportional to the correlator of affinely deformed density pattern in the reference state $S_0(\boldsymbol{\lambda}\cdot\mathbf{q})$ which strongly depends on network preparation conditions:

1) In case of cross-linking in a melt the density fluctuations are suppressed and $S_0(\mathbf{q}) = 0$. The fact that $v(\mathbf{q})$ does not vanish tells us that even though there are no density fluctuations, there are still finite inhomogeneities of cross-link density, which can be revealed upon swelling.

2) For instantaneous cross-linking of a semi-dilute polymer solution $S_0(\mathbf{q})$ is given by the Ornstein–Zernicke expression [19]

$$S_0(\mathbf{q}) = \langle|\delta\tilde{\rho}_0(\mathbf{q})|^2\rangle_0 = \frac{\overline{\rho}_0 N}{B_0\overline{\rho}_0 N + Q^2/2}, \quad (24)$$

which is finite for any second virial coefficient B_0 at network preparation conditions.

3) In case of chemical cross-linking the full structure factor of the gel in the state of preparation is given by that of a polymer liquid, Eq. (24), with $B_0 \to B_0 \to (\overline{\rho}_0 N)^{-1}$. The difference is because some of the monomers act as cross-links, giving additional attraction contribution to the second virial coefficient. The amplitude of heterogeneities grows when approaching the *cross-link saturation threshold* at $B_0\overline{\rho}_0 N = 1$ at which the structure factor $S_0(\mathbf{q} \to 0)$ and the charac-

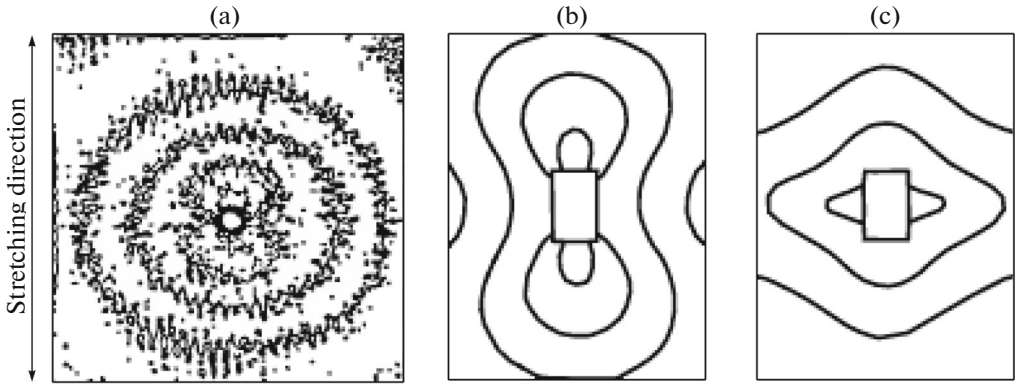

Fig. 3. (a) Typical abnormal butterfly pattern observed in uniaxially stretched (in the direction indicated by the arrows) NIPA/AAc gel. Theoretically predicted scattering function $S(\mathbf{q})$: (b) scattering on variations of the total density ("butterfly"); (c) scattering on deuterated fragments of the network strands ("lozenge").

teristic size of heterogeneities at preparation conditions

$$\xi \cong R/\sqrt{B_0\bar{\rho}_0 N - 1}$$

diverge [19].

Scattering intensity. The scattering intensity on wavevector $\mathbf{q}$ is proportional to the structure factor, which is given by the sum

$$S(\mathbf{q}) = \overline{\langle|\tilde{\rho}(\mathbf{q})|^2\rangle} = \tilde{D}(\mathbf{q}) + \tilde{C}(\mathbf{q}), \qquad (25)$$

of contributions of the thermal fluctuations, Eq. (22), and the inhomogeneous equilibrium density variations due to defects of the topological structure of the network

$$\tilde{C}(\mathbf{q}) = \overline{|\tilde{\rho}_{eq}(\mathbf{q})|^2} = \frac{v(\mathbf{q})}{[1 + B\tilde{g}(\mathbf{q})]^2}, \qquad (26)$$

where bar means ensemble average.

By uniaxially stretching a gel, an increase in the scattered intensity at low q is observed in the stretching direction, which is enveloped by elliptical patterns at larger values of q with maximum oriented normal to this axis. This behavior is opposite to that expected by the theories assuming only thermal fluctuations and called "abnormal butterfly patterns", see Figs. 3a, 3b. These elliptical patterns at large wavevector q originate from the correlator of static inhomogeneities, Eqs. (26) and (23), which contains the term $S_0(\lambda \cdot \mathbf{q})$ that "remembers" the affinely deformed inhomogeneous structure of the network. The butterfly patterns along the stretching axis in the small q range are due to strong angular dependence of the thermal structure factor, Eq. (21). This function comes into numerator of the thermal correlator in Eq. (22), describing "normal butterfly patterns". At high cross-link concentrations the correlator of static inhomogeneities gives the main contribution to the scattering intensity. Since the function $\tilde{g}(\mathbf{q})$ comes into denominator of Eq. (26), this expression describes "abnormal butterfly patterns". As a result, under uniaxial extension, a crossover occurs from normal to abnormal butterfly scattering patterns with increase of the strength of inhomogeneity or the swelling ratio [28]. In addition to such butterfly scattering patterns we also predicted "Lozenge" patterns (see Fig. 3c) if only a part of all network chains, i.e. their deuterated fragments can scatter neutrons, in accord with scattering experiments [29].

The static inhomogeneity in poly(*N*-isopropyl acrylamide) gel (PNIPA) has been investigated in Ref. [30] by using small-angle neutron scattering (SANS) and neutron spin echo. The scattering amplitude $S(q)$ obtained by SANS has been successfully decomposed into thermal and static components, respectively, $\tilde{D}(q)$ and $\tilde{C}(q)$ in Eq. (25). It was revealed that $\tilde{C}(q)$ becomes dominant in the q-region where the abnormal butterfly scattering is observed under stretching. As the temperature increases toward the temperature for volume phase transition, $\tilde{C}(q)$ of a squared Lorentzian shape increases more drastically than $\tilde{D}(q)$ of a Lorentzian shape. These experimental findings are also well described in the theoretical framework of this section.

In Ref. [31] gels prepared by two methods of cross-linking were studied using SANS technique. One is chemical cross-linking with BIS and the other is gamma-ray cross-linking of a PNIPA solution. It is shown that the degree of the inhomogeneity is much larger in the chemically cross-linked gels than in the gamma-ray cross-linked gels, and experimental data are in quantitative agreement with predictions of our theory for scattering intensity $S(\mathbf{q})$ on chemically and instantaneously cross-linked gels, respectively.

The spatial inhomogeneity in poly(acrylamide) (PAAm) gels has been investigated with the static light scattering technique in [32]. A critical polymer network concentration was found at which the degree of the inhomogeneity in PAAm gels attains a maximum

value. This maximum is predicted by the theory presented in this section and can be explained as a result of two opposite effects of the initial monomer concentration on the gel inhomogeneity. Increasing monomer concentration increases both the effective cross-link density and the polymer concentration of the hydrogels. While the inhomogeneity becomes larger due to the first effect, the latter effect decreases the apparent gel inhomogeneity. The interplay of these two opposite effects determines the spatial inhomogeneity in PAAm gels.

Heterogeneities in charged gels. A study of the structure factor of weakly charged polyelectrolyte gels under uniaxial stretching was carried out by Mendes et al. [33], who observed after introducing ions to the gel a disappearance of the butterfly pattern and an increase in scattering intensity in the direction perpendicular to the stretching. The origin of this maximum has been elucidated in SANS experiment by Shibayama et al. on weakly charged polymer PNIPA/AAc gels in deformed state [34]. An anisotropic scattering maximum is observed in this experiment indicating that the spatial distribution of the charged groups changes by gel deformation and therefore, is strongly coupled with the static inhomogeneities.

All the observed patterns of SANS intensity were well reproduced using generalization of the above theory to the case of charged polymer networks [21]. The only effect of electrostatic interactions is to replace the second virial coefficients B_0 and B by effective virial coefficients. This has to be done for both the final state and for the state of preparation:

$$B \to B(\mathbf{q}) \equiv B + 1/s^{DH}(\mathbf{q}),$$

$$B_0 \to B_0(\mathbf{q}) \equiv B_0 + 1/s_0^{DH}(\mathbf{q}),$$

where

$$\frac{1}{s^{DH}(\mathbf{q})} = \frac{4\pi l_B f^2}{\kappa^2 + q^2},$$

is the inverse of the Debye-Hückel structure factor, κ^{-1} is the Debye screening length, f is degree of ionization (fraction of charged monomers) and l_B is the Bjerrum length. $s_0^{DH}(\mathbf{q})$ is obtained by substituting $\kappa = \kappa_0$ and $f = f_0$ into the above equation. As shown in [35] the above theoretical prediction for $S(\mathbf{q})$ well reproduces the observed scattering intensity functions of weakly charged PNIPA/AAc gels.

The new and unexpected results obtained in [21] concern the existence of finite wavelength instabilities in the gel, associated with the onset of microphase separation. What distinguishes between microphase separation in gels and in other (complex fluid) systems is the fact that while in the latter the appearance of a peak in the scattering profile reflects the enhancement of thermal fluctuations about the homogeneous equilibrium state of a liquid, in gels the phenomenon is associated with the reorganization of the local structure of an inhomogeneous solid and the appearance of a spatial modulation in the equilibrium density profile at a wavelength $2\pi/q^*$, even before the onset of the microphase separation transition. The random inhomogeneous density distribution is reconstructed into a new equilibrium profile which can be described as a linear combination of plane waves the amplitudes of which are peaked about $|\mathbf{q}| = q^*$. The transition leads to the formation of lamellar domains, each of which is characterized by a different orientation of the lamellar planes. Under uniaxial deformation, the "directors" of the domains become oriented along the principal axes of compression. Since periodic static density variations lead to the formation of permanent dipole moments, similar effects can be obtained by the application of electric fields.

In general, an introduction of cross-links to a polymer solution leads to an increase in the scattering intensity due to static inhomogeneities. However, a reverse phenomenon, called the "inflection" in scattering intensity, was predicted by the above theory [36] and observed in weakly charged gels and polymer solutions [37]. While the gel becomes more inhomogeneous with increasing the degree of cross-linking in a good solvent, the inhomogeneities can be suppressed in a poor solvent, although in relatively small region of cross-link concentration. However, this phenomenon is interesting due to its physical significance.

Scaling Theory of Heterogeneities

Strong thermal fluctuations in good solvents lead to the breakdown of the mean field approach used in previous sections. Below we adapt this approach using the well-known de Gennes blob picture of semi-dilute solutions [38] and obtain a scaling description [39, 40] of heterogeneities in gels in good solvents. The key idea is the spatial scale separation: while static density inhomogeneities exist only on scales comparable to or larger than the monomer fluctuation radius R, thermal density fluctuations are dominated by smaller scales and are quite similar to those in semi-dilute polymer solutions.

Consider a gel prepared by random cross-linking of chains in a semi-dilute polymer solution in a good solvent at the monomer density ρ_0 that is swollen to density $\rho < \rho_0$. We have to consider monomer density fluctuations in both the initial (where the gel was prepared) and the final (where it is being studied) states of the gel.

On length scales smaller than the correlation lengths

$$\xi_0 = b^{-5/4}\bar{\rho}_0^{-3/4} \quad \text{and} \quad \xi = b^{-5/4}\bar{\rho}^{-3/4}, \qquad (27)$$

density fluctuations are large and the gel behaves as a polymer solution ("liquid-like" regime). On scales larger than the blob size (i.e., for wave vectors $q_0 = 1/\xi$

and $q = 1/\xi$), density fluctuations are small and we can use our mean field description, with appropriately renormalized parameters [19]

$$b_0 \to b_0^{\rm fp} = b(\bar{\rho}_0 b^3)^{-1/8}, \quad (28)$$

$$b \to b^{\rm fp} = b(\bar{\rho} b^3)^{-1/8}, \quad \lambda_k \to \lambda_k b_0^{\rm fp}/b^{\rm fp} \quad (29)$$

where the subscript fp stands for "fixed point" values that differ from the "bare" ones. The renormalized second virial coefficients $B_0^{\rm fp}$ and $B^{\rm fp}$ were calculated in reference [19]:

$$B_0 \to B_0^{\rm fp} = b^3(\bar{\rho}_0 b^3)^{1/4}, \quad B \to B^{\rm fp} = b^3(\bar{\rho} b^3)^{1/4}. \quad (30)$$

Eqs. (27)–(30) complete our discussion of the renormalization of our model: in order to describe a gel in a good solvent on length scales larger than the thermal correlation length, we only have to replace the bare parameters in the previously derived expressions for the free energy, correlation functions, etc., by their renormalized values.

At the equilibrium swelling ($\rho = \rho_{\rm eq}$) in the absence of additional deformations the total free energy of the gel per chain is:

$$A_{\rm ch} = A_{\rm ch}^{\rm os} + A_{\rm ch}^{\rm el} \cong k_{\rm B}T[N(\rho_{\rm eq} b^3)^{5/4} + (\rho_0/\rho_{\rm eq})^{5/12}], \quad (31)$$

and it is minimized at the density [41]

$$\rho_{\rm eq} \cong \frac{(\rho_0 b^3)^{1/4}}{b^3 N^{3/5}}, \quad (32)$$

corresponding to maximum swelling ratio

$$\lambda_{\rm eq} = (\rho_0/\rho_{\rm eq})^{1/3} \cong (\rho_0 b^3)^{1/4} N^{1/5}. \quad (33)$$

Note that similar expression for $\lambda_{\rm eq}$ is obtained in mean field model of a gel with second virial coefficient $B \cong b^3$.

AMPLIFICATION OF CROSS-LINKING DENSIRY PATTERN

Below we assume that the gel was initially cross-linked in a polymer melt and then a pre-programmed pattern in cross-link concentration (i.e., a well-defined region of higher cross-link density compared to that of the surrounding network) is created in the network using, say, a light-sensitive cross-linking technique. The free energy of such network is given by Eq. (11) where $G(\mathbf{x}_0)$ is the polymer contribution to the elastic modulus of the cross-linked melt (which is proportional to the local cross-link density)

$$G(\mathbf{x}_0) = \bar{G} + \hat{G}(\mathbf{x}_0), \quad (34)$$

and $\hat{G}(\mathbf{x}_0)$ represents the variations of cross-link density introduced by the second cross-linking step (see Fig. 1a). Notice that the reference state describes a stretched network with inhomogeneous cross-link density but a homogeneous monomer density.

Minimizing the free energy in Eq. (7) with respect to displacements $\mathbf{u}$ at the preparation state (all $\lambda_k = 1$) we find that in a melt the cross-links and the monomers will remain at their previous positions and the elastic reference state will not change after relaxation. We conclude that information about the pattern written on network structure is hidden in preparation state and can only be revealed after swelling.

Equilibrium Density Profile

Below we analyze how density pattern deforms under several different solvent conditions.

Good solvent: unentangled gel. The equilibrium deformation of the deformed gel with given cross-link density pattern $\hat{G}(\mathbf{x})$ is found by minimizing its free energy, Eq. (11). The solution of differential equation for minimum condition [42]

$$\frac{\Delta\rho(\mathbf{x})}{\bar{\rho}} \cong -\Sigma_k \frac{\partial u_k(\mathbf{x})}{\partial x_k} = \Sigma_k \lambda_k^2 \frac{\partial^2}{\partial x_k^2} \int g[\gamma^{-1}\cdot(\mathbf{x}-\mathbf{y})]\hat{G}(\lambda^{-1}\cdot\mathbf{x})\frac{d\mathbf{y}}{\Pi_k \gamma_k}, \quad (35)$$

can be expressed through Green's functions of the Laplace equation in 2 and 3 dimensions, respectively:

$$g_{2D}(\mathbf{x}) = \frac{1}{4\pi}\ln \Sigma_k x_k^2, \quad g_{3D} = -\frac{1}{4\pi\sqrt{\Sigma_k x_k^2}}. \quad (36)$$

Here we defined

$$\gamma_k^2 = \bar{G}\lambda_k^2 + K^{\rm os}. \quad (37)$$

In case of isotropically stretched/swollen gel with all $\lambda_k = \lambda$ the equilibrium monomer density depends on local cross-link concentration,

$$\frac{\Delta\rho(\mathbf{x})}{\bar{\rho}} = \frac{\lambda^2}{\gamma^2}\hat{G}\left(\frac{\mathbf{x}}{\lambda}\right). \quad (38)$$

We conclude that under isotropic deformation, the monomer density in a swollen gel produces an undistorted, uniformly stretched image of the pattern of cross-link density originally "written" on the homogeneous network (compare Figs. 1a and 1c).

Equilibrium displacement is expressed through the variation of monomer density, Eq. (38), as

$$u_k(\mathbf{x}) = -\frac{\partial}{\partial x_k}\int g(\mathbf{x}-\mathbf{y})\frac{\Delta\rho(\mathbf{y})}{\bar{\rho}}d\mathbf{y}. \quad (39)$$

We conclude that although density variations in isotropically deformed gels are strictly local, there is long-range strain field decaying as power law of the distance $|\mathbf{x}-\mathbf{y}|$. This strain induces a stress distribution in the gel, which can be observed by measuring the birefringence of transmitted light (stress-optical law [43]).

In anisotropically deformed networks the pattern is strongly distorted (compare Figs. 1a, 1d) and $\tilde{\rho}(\mathbf{x})$ decays as power law of a distance $|\mathbf{x}-\mathbf{y}|$ from the localized cross-link density inhomogeneity $\tilde{G}(\mathbf{y})$. Observe that variations of monomer density are largest along the direction of stretching. This effect is closely related to the well known "butterfly" picture (see Fig. 3) in contour plots of neutron scattering from random inhomogeneities of network structure in anisotropely deformed swollen gels (see section *Random Heterogeneities* and [44]).

Our consideration can also be extended to describe patterns obtained by cross-linking a semi-dilute polymer solution with free energy calculated in section *Scaling Theory of Heterogeneities*. Since both elastic and osmotic terms in the gel free energy are multiplied by the same scaling factor $(\rho/\rho_0)^{1/4}$ scaling renormalization of free energy does not change the results obtained for the mean field model. We conclude that density patterns such swollen gels deform affinely (non-affinely) under isotropic (anisotropic) deformation, just like in the case of cross-linking in the melt.

Good solvent: entangled gel. The entanglement contribution to the free energy, Eq. (11), can be simplified in the most interesting case of isotropic deformation [45]:

$$\Delta A_e = \int \frac{\bar{G}_e}{2} \Sigma_{kl} \lambda \left(\frac{\partial u_k}{\partial x_l} \right)^2 \frac{d\mathbf{x}}{\lambda^3}. \quad (40)$$

The entanglement elastic modulus, $\bar{G}_e \cong k_B T \bar{\rho}/N_e$ (see Eq. (18)), is proportional to density of entanglements, $\bar{\rho}/N_e$ (N_e is number of monomers between neighboring entanglements). Repeating the calculations that led to Eq. (38), we find the equilibrium monomer density

$$\frac{\Delta\rho(\mathbf{x})}{\bar{\rho}} = \frac{\lambda^2}{\bar{G}\lambda^2 + \bar{G}_e\lambda + K^{os}} \hat{G}\left(\frac{\mathbf{x}}{\lambda}\right). \quad (41)$$

We conclude that entanglements reduce the monomer density contrast, and that their contribution decreases with increasing stretching factor λ. The latter effect originates in the slippage of entanglements towards to the permanent crosslinks in strongly stretched networks [45]. In case of large network deformation $\lambda > N/N_e$, the confinement due to entanglements is not important since the local entanglements do not "exist" anymore.

θ-Solvent. In a θ-solvent the second virial coefficient vanishes ($B = 0$) and Eq. (35) reproduces without distortion affinely stretched initial pattern

$$\Delta\rho(\mathbf{x})/\bar{\rho} = \hat{G}(\lambda^{-1} \cdot \mathbf{x})/\bar{G}. \quad (42)$$

Small deviations from affinity are expected because of the non-vanishing third virial coefficient. Thus, we show that the pattern always stretches affinely in a θ-solvent, even under anisotropic deformations.

Poor solvent. Strong enhancement of the contrast between the high and the low monomer density regions can be obtained by placing the gel (with fixed boundaries—otherwise it would collapse) in a poor solvent with negative second virial coefficient $B < 0$. In case of very poor solvent with

$$\gamma^2 = \bar{G}\lambda^2 + k_B T B \bar{\rho}^2 < 0, \quad (43)$$

the gel becomes unstable with respect to formation of dense filamentous structures [46]. Below we consider the case of mildly poor solvent close to θ-conditions with small $B < 0$ and positive $\gamma^2 > 0$.

At small γ^2 the amplitude of density variations $\rho(\mathbf{x})$ can be significantly increased because of the small denominator in Eq. (38) and we have to take into account corrections due to second order in $\mathbf{u}$ term

$$\varepsilon(\mathbf{u}) = \Sigma_{kl} \left(\frac{\partial u_k}{\partial x_k} \frac{\partial u_l}{\partial x_l} - \frac{\partial u_k}{\partial x_l} \frac{\partial u_l}{\partial x_x} \right), \quad (44)$$

in expression (Eq. (5)) for monomer density,

$$\rho(\mathbf{x}) = \bar{\rho}/\det(\mathbf{F}^u), \quad (45)$$

where

$$\det(\mathbf{F}^u) = 1 + \Sigma_k \frac{\partial u_k}{\partial x_k} + \varepsilon(\mathbf{u}). \quad (46)$$

To first order in ε we find

$$\frac{\Delta\rho(\mathbf{x})}{\bar{\rho}} \cong \frac{\lambda^2}{\gamma^2} \left[\hat{G}\left(\frac{\mathbf{x}}{\lambda}\right) - \bar{G}\varepsilon(\mathbf{u}) \right], \quad (47)$$

where the equilibrium displacement in $\varepsilon(\mathbf{u})$ is determined as

$$u_k(\mathbf{x}) \cong -\frac{\lambda^2}{\gamma^2} \frac{\partial}{\partial x_k} \int g(\mathbf{x}-\mathbf{y}) \hat{G}\left(\frac{\mathbf{y}}{\lambda}\right) d\mathbf{y}. \quad (48)$$

We conclude that the correction term in Eq. (47) may significantly enhance the contrast between the high and the low monomer density regions of the profile (Fig. 4). This effect is most pronounced near the corners of the pattern where several edges converge and it leads to distortion of the otherwise affinely stretched profile at these points.

We conclude that when the amplitude of cross-link density variations is sufficiently low, the image stretches affinely with the isotropic deformation but that for larger density contrasts the image becomes distorted, especially near the edges and corners of the pattern.

Contribution of Random Heterogeneities

Frozen-in random heterogeneities of network structure can change the image beyond recognition [47]. The free energy of a gel with frozen-in heterogeities was derived in [20]. The only source of het-

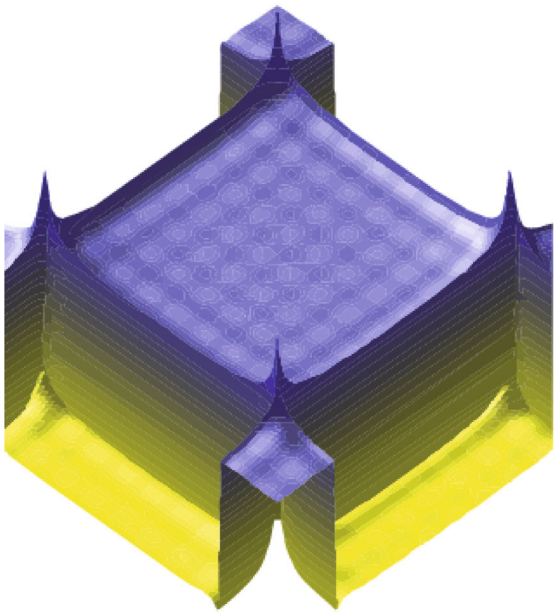

Fig. 4. (Color online) Density profile in poor solvent for initial cross-link concentration profile shown in Fig. 1a.

erogeneities in the melt with fixed monomer density is statistical distribution of cross-links in the state of preparation that arises as the consequence of the random process of cross-linking. This frozen-in distribution is described by an additional contribution to the free energy, see Eq. (13):

$$\Delta A^{\text{rand}} = -\int \mathbf{f}^{\text{rand}}(\mathbf{x})\mathbf{u}(\mathbf{x})d\mathbf{x}, \qquad (49)$$

where $f^{\text{rand}}(\mathbf{x})$ is density of random Gaussian force, characterized by correlation function given by Eq. (17). Comparing the amplitude of frozen-in fluctuations on a scale $r \gg R$ with variations of elastic modulus $\hat{G}$ on this scale we conclude that the contribution of frozen-in heterogeneities can be neglected if

$$\hat{G}/\bar{G} \approx 1/(\bar{c}r^3)^{1/2}, \qquad (50)$$

where $\bar{c}$ is average cross-link concentration and thus, frozen-in heterogeities have no influence on large-scale patterns. The suppression of frozen-in heterogeneities of monomer density is due to strong overlap of network chains on scales $r \gg R$ [48].

DISCUSSION

We studied the combined effect of swelling and deformation on inhomogeneous networks, prepared by cross-linking a melt and semidilute solution of polymer chains. It is well-known that cross-link density heterogeneities that have no effect on the monomer density in the state of preparation (a melt or a concentrated polymer solution), can be revealed by swelling the gel and observing the enhancement of light, X-ray and neutron scattering from the resulting monomer density inhomogeneities [49–52]. In this paper we focused on a related phenomenon, namely that when large-scale cross-link density patterns are written into the network structure, the hidden image can be revealed by swelling and stretching the gel and observing the corresponding patterns of monomer density. The predicted effect has been observed in computer simulations of networks with non-uniform concentration of cross-links: see Figs. 11 and 13 in [53].

Using the mean field theory of elasticity of polymer gels we showed that stretching/swelling in good solvent acts as a magnifying glass: while isotropic stretching reproduces an enlarged but otherwise undistorted version of the original pattern, anisotropic stretching distorts this pattern, see Fig. 1.

We compare these results with those obtained for ordinary elastic solids with inhomogeneous elastic moduli and found that in this case even isotropic deformations lead to distorted patterns, see Fig. 1. Physically the difference between elastic energy of a solid and of a gel stems from the fact that while in solids there is a stress-free state of equilibrium (crystal lattice) that minimizes the energy of interaction between the atoms, the equilibrium state of gels is not stress-free. Polymer networks are made of entropic springs and, in the absence of osmotic pressure due to permeation by good solvent or due to excluded volume interactions in the melt state, such networks would collapse to the size of a single spring. The finite length of entropic springs in the swollen gel is the result of osmotic pressure which can be replaced by equivalent isotropic stretching forces that act on the outer boundaries of the gel [54].

The difference between gels and solids becomes apparent when considering two simple toy models of heterogeneous gel and solid as two Hookean springs with moduli k_1 and k_2, connected in series as in Fig. 5:

a) Gel model. Osmotic pressure is represented by a force f^{os} applied to free ends of the connected springs. Since we want to model a gel with spatially-varying of density of cross-links, in which there are two different average lengths of chains between cross-links, the spring constants of the corresponding entropic springs are different, $k_1 \neq k_2$. The equilibrium lengths of the Gaussian springs, $r_1^{\text{eq}} = f^{\text{os}}/k_1$ and $r_2^{\text{eq}} = f^{\text{os}}/k_2$, are entirely determined by the osmotic force that isotropically stretch the "gel". If we apply additional force f, each of the springs will deform affinely with distance $r_1 + r_2$ between the ends to which the force is applied ("boundaries" of the system):

$$r_1 = \lambda r_1^{\text{eq}}, \quad r_2 = \lambda r_2^{\text{eq}}, \quad \lambda = \frac{r_1 + r_2}{r_1^{\text{eq}} + r_1^{\text{eq}}}. \qquad (51)$$

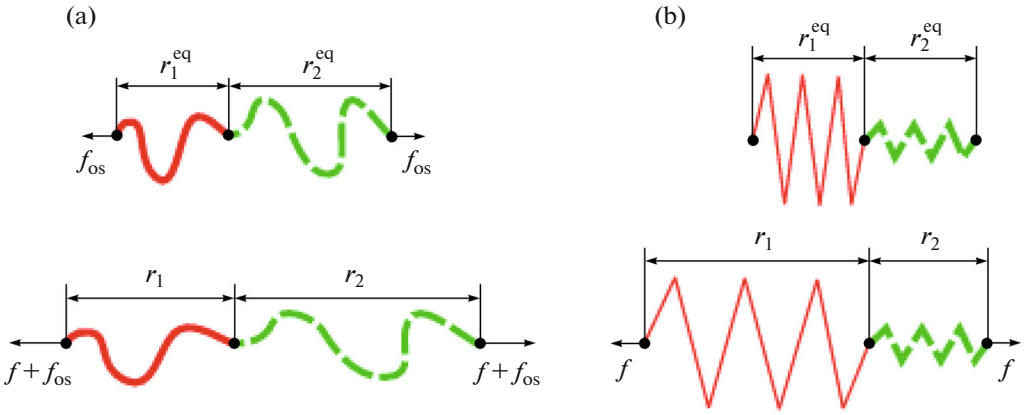

Fig. 5. (Color online) Two springs models, demonstrating (a) affine deformation of gels and (b) non-affine deformation of solids.

b) Solid model. The springs of a "solid" have equilibrium lengths r_1^{eq} and r_2^{eq} even in the stress-free state. During stretching due to force f applied to the ends of the two-spring system, such a solid deforms non-affinely:

$$r_1 = r_1^{eq} + (\lambda - 1)(r_1^{eq} + r_2^{eq})\frac{k_2}{k_1 + k_2},$$
$$r_2 = r_2^{eq} + (\lambda - 1)(r_1^{eq} + r_2^{eq})\frac{k_2}{k_1 + k_2} \quad (52)$$

with the soft spring ($k_1 < k_2$) stretched more than the rigid one.

These two simple toy models illustrate why under isotropic deformations, cross-linking density patterns in gels are stretched affinely, whereas soft regions in solids would undergo larger deformation compared to more rigid regions, thus distorting the original pattern.

CONCLUSIONS

Over the past twenty years, basic problems of gels description have been elucidated, such as change of strands conformations during swelling/deswelling, dynamics of phase transitions in gels [55] and soon. Although from the very beginning the heterogeneities were recognized as one of the most essential features of gels [56], it took long time to formulate their theoretical description due to complexity of this problem. Up to today, the understanding of the gel structure has greatly improved owing to both theoretical developments and a large number of experimental studies. Effect of cross-links on heterogeneous structure of polymer gels, abnormal butterfly patterns, microphase separation, and so on, are well understood with the aid of the approaches discussed in this paper. However, many questions still remain unsolved, such as deformation mechanism of heterogeneous super-tough networks, kinetics of crack growth and phase transitions in such networks. And we hope that the proposed approaches can help to answer these questions in the near future.

Finally, we would like to comment on possible applications of our results. In most applications involving gels such as biomimetic sensors, actuators and artificial muscles [57], macroscopically inhomogeneous (layered) gels undergo shape transitions when the thermodynamic conditions are changed or in response to application of external fields [58].

In case of internally heterogeneous networks, the cross-link density pattern imprinted into the gel structure by, say, activation of light-sensitive cross-links (or alternatively, using hydrogels cross-linked by complementary ssDNA chains whose local elastic properties can be modified by binding ligands, viruses, etc. to these physical cross-links [59, 60]), can be microscopic (micron size) and therefore would have little effect on the shape of the gel. Upon swelling and/or isotropic stretching in good solvent, the magnified density pattern can be imaged on a light-sensitive screen.

The contrast can be significantly enhanced by stretching the entire gel in poor solvent. Gel boundaries should be fixed in order to avoid contraction of the gel. Gel contraction can also be prevented by focusing a laser beam only on a part of the localized pattern and heating it, resulting in local change of the quality of solvent. Although kinetics of shape transitions in the bulk gel is very slow, the laser beam scanning speed can be high enough since relaxation time of the spot of a small size $r > R$ is very short, $\tau_R \cong r^2/D$. Here D is the collective diffusion constant introduced by Tanaka et al. [61], $D = (4\bar{G}/3 + K^{os})/\zeta$, where ζ is the friction coefficient between network and solvent. The image contrast can be adjusted during the "reading" by varying the heating power.

The sensitivity of the image to quality of solvent can be useful for sensor devices. The distortion under anisotropic deformation disappears in θ-solvent, whereas the pattern distortion in a poor solvent can be used in image edge detection technique.

One of the most important contributions of Sam Edwards was an understanding that it is not enough to rely on the government to provide the resources for new researches. Rather, best way to initiate the research was to become much more closely associated with the needs of industry.

Sam Edwards contributions to physics in general were immense. He involved many people into his projects, remaining approachable to all his colleagues and students. And he managed to engage senior figures in industry and government due to hosting dinners were people came in contact being delighted with his magnificent wine collection.

REFERENCES

1. S. F. Edwards, Proc. Phys. Soc., London **85**, 613 (1965).
2. S. F. Edwards, Proc. Phys. Soc., London **88**, 625 (1966).
3. S. F. Edwards, J. Phys. A: Gen. Phys. **1**, 15 (1968).
4. S. F. Edwards, Proc. Phys. Soc., London **92**, 9 (1967).
5. M. Doi and S. F. Edwards, J. Chem. Soc., Faraday Trans. 2 **74**, 1789 (1978).
6. P. G. de Gennes, J. Chem. Phys. **55**, 572 (1971).
7. R. T. Deam and S. F. Edwards, Philos. Trans. R. Soc. London, Ser. A **280**, 317 (1976).
8. F. Di Lorenzo and S. Seiffert, Polym. Chem. **6**, 5515 (2015).
9. J. Bastide (private communication) (1986).
10. T. A. Vilgis and G. Heinrich, Angew. Makromol. Chem. **202/203**, 243 (1992).
11. T. A. Vilgis, J. -U. Sommer, and G. Heinrich, Makromol. Symp. **93**, 205 (1995).
12. C. Svaneborg, G. S. Grest, and R. Everaers, Polymer **46**, 4283 (2005).
13. Yu. Ya. Gotlib, A. A. Gurtovenko, and H.-G. Kilian, Polym. Sci., Ser. A **43**, 308 (2001).
14. S. V. Panyukov, Sov. Phys. JETP **61**, 1065 (1985).
15. S. V. Panyukov, Sov. Phys. JETP **67**, 930 (1988).
16. S. V. Panyukov, JETP Lett. **55**, 608 (1992).
17. S. V. Panyukov, Sov. Phys. JETP **69**, 342 (1989).
18. S. V. Panyukov, JETP Lett. **58**, 118 (1993).
19. S. Panyukov and Y. Rabin, Phys. Rep. **269**, 1 (1996).
20. S. Panyukov and Y. Rabin, Macromolecules **29**, 7960 (1996).
21. S. Panyukov and Y. Rabin, Macromolecules **30**, 301 (1997).
22. S. V. Panyukov and I. I. Potemkin, Polym. Sci. USSR **36** (1), 115 (1994).
23. S. Panyukov and I. Potemkin, J. Phys. I **7**, P1 (1997).
24. R. S. Stein, J. Polym. Sci. B **7**, 657 (1969).
25. S. Mallam, F. Horkay, A. M. Hecht, and E. Geissler, Macromolecules **22**, 3356 (1989).
26. E. M. Lifshitz, A. Yu. Grosberg, and A. R. Khokhlov, Rev. Mod. Phys. **50**, 683 (1978).
27. P.-G. de Gennes, J. Phys., Lett. **40**, 69 (1979).
28. A. Onuki, J. Phys. II **2**, 1155 (1992).
29. S. V. Panyukov, Sov. Phys. JETP **75**, 347 (1992).
30. S. Koizumi, M. Monkenbusch, D. Richter, D. Schwahn, and B. Farago, J. Chem. Phys. **121**, 12721 (2004).
31. T. Norisuye, N. Masui, Y. Kida, M. Shibayama, D. Ikuta, E. Kokufuta, S. Ito, and S. Panyukov, Polymer **43**, 5289 (2002).
32. M. Y. Kizilay and O. Okay, Macromolecules **36**, 6856 (2003).
33. E. Mendes, F. Schosseler, F. Isel, F. Boué, J. Bastide, and S. J. Candau, Europhys. Lett. **32**, 273 (1995).
34. M. Shibayama, K. Kawakubo, F. Ikkai, and M. Imai, Macromolecules **31**, 2586 (1998).
35. M. Shibayama, K. Kawakubo, and T. Norisuye, Macromolecules **31**, 1608 (1998).
36. M. Shibayama, F. Ikkai, Y. Shiwa, and Y. Rabin, J. Chem. Phys. **107**, 5227 (1997).
37. F. Ikkai, M. Shibayama, and C. C. Han, Macromolecules **31**, 3275 (1998).
38. P. -G. de Gennes, *Scaling Concepts in Polymer Physics* (Cornell Univ. Press, Ithaca, New York, 1979).
39. S. V. Panyukov, Sov. Phys. JETP **71**, 372 (1990).
40. S. V. Panyukov and S. I. Kuchanov, Polym. Sci. USSR **32** (4), 682 (1990).
41. S. V. Panyukov, JETP Lett. **46**, 595 (1987).
42. S. Panyukov and Y. Rabin, Macromolecules **48**, 7378 (2015).
43. M. Doi and S. F. Edwards, *The Theory of Polymer Dynamics* (Clarendon, Oxford, 1986).
44. J. Bastide, L. Leibler, and J. Prost, Macromolecules **23**, 1831 (1990).
45. M. Rubinstein and S. Panyukov, Macromolecules **35**, 6670 (2002).
46. O. Peleg, M. Kröger, I. Hecht, and Y. Rabin, Europhys. Lett. **77**, 58007 (2007).
47. O. Peleg, Y. Rabin, and M. Kroger, Phys. Rev. E **79**, 040401 (2009).
48. M. Rubinstein and R. H. Colby, *Polymer Physics* (Oxford Univ. Press, Oxford, 2003).
49. S. Candau, J. Bastide, and M. Delsanti, Adv. Polym. Sci. **44**, 27 (1982).
50. F. Horkay, A.-M. Hecht, S. Mallam, E. Geissler, and A. R. Rennie, Macromolecules **24**, 2896 (1991).
51. M. Shibayama, T. Tanaka, and C. C. Han, J. Chem. Phys. **97**, 6829 (1992).

52. J. Bastide and S.Candau, in *The Physical Properties of Polymeric Gels*, Ed. by J. P. Cohen Addad (Wiley, New York, 1996), p. 143.
53. M. Lang, D. Goritz, and S. Kreitmeier, in *Constitutive Models for Rubber III*, Ed. by J. Busfield and A. Muhr (Balkema Publ., Leiden, 2003), pp. 195–202.
54. P. J. Flory and J. Rehner, J. Chem. Phys. **11**, 521 (1943).
55. A. Onuki, *Phase Transition Dynamics* (Cambridge Univ. Press, Cambridge, 2004).
56. J. Bastide and L. Leibler, Macromolecules **21**, 2647 (1988).
57. M. Shahinpoor, Y. Bar-Cohen, J. O. Simpson, and J. Smith, Smart Mater. Struct. **7**, R15 (1998).
58. Y. Klein, E. Efrati, and E. Sharon, Science **315**, 1116 (2007).
59. J. Shin, A. G. Cherstvy, and R. Metzler, Phys. Rev. X **4**, 021002 (2014).
60. J. Liu, H. Liu, H. Kang, M. Donovan, Z. Zhi, and W. Tan, Anal. Bioanal. Chem. **402**, 187 (2012).
61. T. Tanaka and D. J. Filmore, J. Chem. Phys. **70**, 1214 (1979).